JOURNAL OF SOLID STATE CHEMISTRY 36, 339–348 (1981)

Preparation and Mössbauer Studies of $(Fe_yNb_{1-y})_{1+x}S_2$ Compounds

MASATAKA WAKIHARA, HIROFUMI HINODE, MASANORI ABE,* AND MASAO TANIGUCHI

*Department of Chemical Engineering, Tokyo Institute of Technology, Ookayama, Meguro-ku, Tokyo 152 Japan, and *Department of Physical Electronics, Tokyo Institute of Technology, Ookayama, Meguro-ku, Tokyo 152 Japan*

Received April 14, 1980; in revised form August 4, 1980

The phase relations for iron niobium sulfides $(Fe_yNb_{1-y})_{1+x}S_2$ have been examined by varying the partial pressure of sulfur at 950°C. While niobium is difficult to dissolve in iron sulfide, iron dissolves in niobium sulfide up to about 35% of the total metal sites. Iron niobium sulfide has the layered hexagonal type structure ($2s$–$Nb_{1+x}S_2$) with change in the lattice parameters depending on both the value of x and the amount of the iron dissolved. The Mössbauer spectra of sulfides with three different Fe/Nb ratios, 1/9 (y = 1/10), 1/4 (y = 1/5), and 1/2 (y = 1/3) were taken at 77 and 295 K. Each spectrum is composed of a quadrupole doublet which can be attributed to the Fe^{2+} ions in high spin state. The quadrupole splitting at 295 K decreases markedly with decrease in x which is related to change of the lattice parameters. Fe atoms cannot enter at random into all metal sites, and prefer to intercalate in the sites of partially filled layers. Possible models for the cation distribution in each metal layer are discussed.

Introduction

A number of transition metal chalcogenides form compounds with layered structure in which a hexagonal array of metal atoms is sandwiched between two hexagonal layers of chalcogen atoms. The weak van der Waals bonding between chalcogen atoms of adjacent X–M–X layers allows easy insertion or intercalation of atoms between the layers. There has been considerable interest in the metal intercalation compounds of the dichalcogenides recently, because of their potential use as cathodes in high energy density secondary batteries (*1*).

Niobium disulfide, in which the metal has trigonal prismatic coordination to sulfur, is particularly noteworthy as a host material for such intercalation compounds. So far there have been several electrochemical and crystallographic investigations for NbS_2 intercalated with alkali (*1, 2*) and transition metals (*2–9*). Rouxel *et al.* (*6*) and Boswell *et al.* (*8*) have reported on the structure and the nonstoichiometry of $Fe_x NbS_2$. They prepared the compounds using the vacuum seal technique, and pointed out the existence of superstructures in the ternary system. Rouxel *et al.* (*6*) found the solubility limit of iron in NbS_2 to be 33% of the total metal sites at 950°C.

In the present study, we prepared Fe–Nb–S ternary compounds corresponding to $(Fe_yNb_{1-y})_{1+x}S_2$ at different partial pressures of sulfur at 950°C and obtained equilibrium isotherms for different y utilizing

0022-4596/81/030339-10$02.00/0

our previous Nb–S equilibrium study (*10*). X-Ray powder diffraction, electron microscope, and Mössbauer spectra studies of the quenched samples were used to examine the relation between structure and the nonstoichiometry, the order–disorder problems of intralayer metal sites and also the behavior of iron atoms in the metal sites. Further, iron distribution in the available metal sites was considered.

Experimental

Material. Niobium sulfides with known composition prepared by a previously described method (*10*) and natural crystalline pyrite (~99.9% Hanaoka Mine, Japan) were mixed in an agate motor with acetone in various Fe/Nb ratios. The mixtures were dried under vacuum without firing and used as starting materials.

Phase equilibria. The experimental technique used for the determination of phase equilibria has been described in our previous work (*10, 11*). An exemplary procedure is as follows; a quartz crucible containing about 200 mg of the starting material was suspended in a vertical furnace with a controlled current of H_2–H_2S gas mixture or sulfur vapor with nitrogen carrier gas. After equilibration between gas and condensed phases, the specimen was quenched to about 0°C. The chemical composition of the powdered sample was determined by the change in weight on oxidation in air to a Fe_2O_3–Nb_2O_5 mixture at 700°C. The quenched sulfides were identified by their X-ray powder diffraction patterns using V-filtered Cr$K\alpha$ radiation.

Electron micrographs and electron diffraction spots for the sulfide $Fe_{1/2}NbS_2$ were taken by a high resolution electron microscope (JEM-200C).

Mössbauer spectra. Mössbauer spectra were taken with a conventional constant acceleration spectrometer using 5 mCi of ^{57}Co in an Rh matrix as the source. The velocity scale was calibrated on a standard $Na_2[Fe(CN)_5NO] \cdot 2H_2O$ absorber and the center shift was referred to a 310 stainless-steel absorber. The measurement was performed for specimens at 295 K (for $y = \frac{1}{10}$, $\frac{1}{5}$, and $\frac{1}{3}$) and at 77 K (for $y = \frac{1}{3}$), using powdered samples suspended on paper with a cellulose adhesive. An exposure time of 3 ~ 10 hr was required to obtain a reliable absorption spectrum, depending on the iron concentration of the samples.

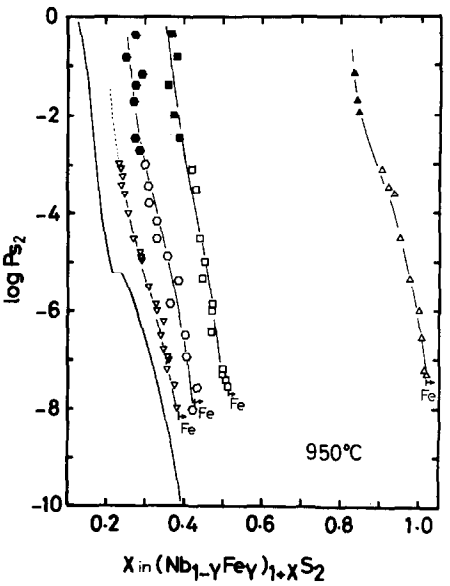

FIG. 1. Equilibrium sulfur pressure–composition isotherms for the Fe–Nb–S system at 950°C. Solid symbols, direct sulfur pressure control method; open symbols, H_2S/H_2 gas mixing method; △, pure Fe–S system; □, $y = 1/3$; ○, $y = 1/5$; ▽, $y = 1/10$ for $(Fe_yNb_{1-y})_{1+x}S_2$.

Results and Discussion

The equilibrium isotherms of the $(Fe_yNb_{1-y})_{1+x}S_2$ system ($y = \frac{1}{10}$, $y = \frac{1}{5}$, and $y = \frac{1}{3}$) and the terminal binary Fe–S system obtained at 950°C in the present study are shown in Fig. 1, together with the isotherm of the terminal Nb–S system previously determined at the same tem-

perature (*10*). The data of composition vs partial pressure of sulfur P_{S_2} are given in Table I. Every isotherm showed nonstoichiometry which increases with decreasing partial pressure of sulfur. The Fe–Nb–S compounds decomposed resulting in release of reduced metallic iron at P_{S_2} below about $10^{-7.5}$ atm depending slightly on the iron amount. Pyrrhotite decomposed to metallic iron and sulfur vapor at a P_{S_2} between $10^{-7.35}$ and $10^{-7.40}$ atm. This agrees well with the estimated value of $10^{-7.42}$ atm from JANAF thermochemical tables. In our previous study of the Nb–S

TABLE I

RELATED VALUES FOR IRON NIOBIUM SULFIDES

Composition X in $M_{1+x}S_2$	Equilibrium pressure $-\log P_{S_2}$ at 950°C	Lattice parameters			Mössbauer (mm/sec)	
		a (Å)	$\frac{1}{2}c$ (Å)	$\frac{1}{2}V$ (Å^3)	C.S.	Q.S.
			$2s$–$(Fe_{1/3}Nb_{2/3})_{1+x}S_2$			
0.515	7.56	3.337	6.185	59.65	0.97	1.00
0.507	7.42	3.334	6.185	59.54	0.96	0.98
0.500	7.19	3.331	6.170	59.28	0.95	0.96
					(1.10)[a]	(1.16)[a]
0.498	7.29	3.334	6.176	59.45	0.98	0.98
0.473	6.43	3.334	6.175	59.44	0.96	0.97
0.455	5.00	3.333	6.155	59.21	0.95	0.89
0.440	4.51	3.331	6.150	59.09	0.93	0.88
0.424	3.10	3.330	6.130	58.86	0.91	0.70
0.382	0.85	3.328	6.099	58.50	0.89	0.45
					(1.00)[a]	(0.51)[a]
			$2s$–$(Fe_{1/5}Nb_{4/5})_{1+x}S_2$			
0.421	8.02	3.325	6.222	59.64	0.98	1.08
0.409	6.94	—	—	—	0.96	1.00
0.386	5.39	3.332	6.188	59.30	0.94	0.88
0.370	5.86	3.331	6.173	59.17	0.95	0.88
0.357	4.90	3.326	6.149	58.90	0.93	0.75
0.329	4.51	3.329	6.130	58.83	0.92	0.69
0.310	3.80	—	—	—	0.91	0.61
0.300	3.00	3.327	6.104	58.51	0.87	0.53
0.252	0.85	3.329	6.065	58.20	0.82	0.17
			$2s$–$(Fe_{1/10}Nb_{9/10})_{1+x}S_2$			
0.383	8.01	—	—	—	0.97	1.16
0.362	6.94	—	—	—	0.97	1.08
0.350	6.80	3.322	6.270	59.92	—	—
0.341	6.50	3.323	6.260	59.86	—	—
0.340	7.29	—	—	—	0.97	1.11
0.330	5.86	—	—	—	0.95	0.95
0.309	5.53	3.326	6.237	59.78	0.97	1.16
0.292	4.95	3.328	6.204	59.51	—	—
0.291	4.90	—	—	—	0.93	0.83
0.234	3.00	—	—	—	0.88	0.43

[a] Data at 77 K.

system (*10*), there were two hexagonal phases, 2s–$Nb_{1+x}S_2$ and 3s–$Nb_{1+x}S_2$ in which repeating units in the *c*-direction are two or three NbS_2 slabs, respectively (*12*). However, nonstoichiometric compounds with the 2s–$Nb_{1+x}S_2$ type structure were the main products in all the quenched samples of the $(Fe_yNb_{1-y})_{1+x}S_2$ system, although a small amount of the 3s–$Nb_{1+x}S_2$ type compound was also obtained for $y = \frac{1}{10}$ at $P_{S_2} > 10^{-3}$ atm. The two structure region is indicated by a dashed line in the isotherm in Fig. 1. By using X-ray powder diffraction patterns, mutual solubility limits of iron to 2s–$Nb_{1+x}S_2$ and niobium to pyrrhotite were obtained, and confirmed by the sulfurization reaction of the samples. It was found that niobium did not dissolve in pyrrhotite within the measurable sensitivity of X-ray diffraction, while iron dissolved in $Nb_{1+x}S_2$ up to 35 mol% of the total metal sites. At 38% iron, a few relic peaks of pyrrhotite were identified. This finding consists with the data obtained from the vacuum seal technique by Rouxel *et al.* (*6*).

In order to clarify the behavior of cations in the layered metal sites, lattice parameters of quenched specimens with the three metallic ratios, $y = 1/10$, $y = 1/5$, and $y = 1/3$, were examined. The hexagonal lattice parameters and the lattice volume for the $(Fe_yNb_{1-y})_{1+x}S_2$ system are shown in Fig. 2 and summarized in Table I. Also included in Fig. 2 are previous data for the Nb–S system (the ordinate scale for the volume in our previous paper (*10*) was erroneous). The lattice constant *a* does not change markedly with variation in *y* over the composition range $\sim 0.25 < x < \sim 0.5$. The lattice constant *c* decreases with decrease in *x*. It also decreases with increase in *y* (or increase of concentration in the metal sites) when the total metal concentration $(1 + x)$ is kept constant. Accordingly, the increase in iron content in the layered

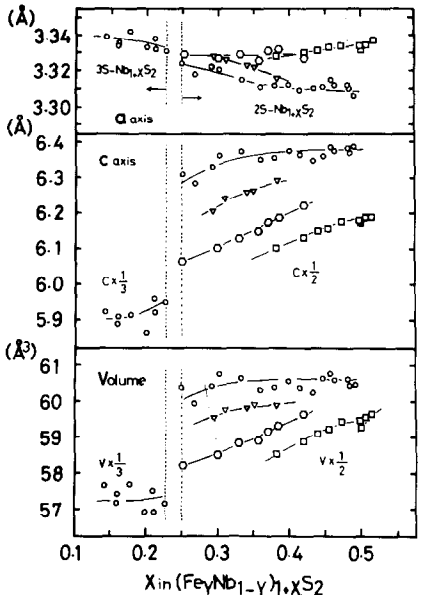

FIG. 2. Plot of lattice parameters and unit cell volume vs composition of quenched iron niobium sulfides. The symbols are the same as in Fig. 1.

metal sites contributes to decreasing the distance of the van der Waals gap. The lattice constant *c* and the lattice volume for $y = 1/3$ (square symbol) show a discontinuity at a composition $x = 0.50$ which corresponds to $(Fe_{1/3}Nb_{2/3})_{1.5}S_2$ or $Fe_{1/2}NbS_2$. By only slight increase of the metal sites up to $x = 0.53$, the 2s–$(Fe_{1/3}Nb_{2/3})_{1+x}S_2$ decomposes to metallic iron and the component sulfides. Details will be discussed later.

Figure 3a shows a typical example of the Mössbauer absorption spectra taken at 295 K. Each spectrum is composed of a paramagnetic quadrupole doublet of asymmetric shape. The asymmetry may be ascribed to the preferred orientation of the polycrystalline sample, since it depended strongly on the preparation method of the absorber. The spectra taken at 77 K are shown in Fig. 3b. They are also paramagnetic doublets, and their quadrupole splitting (Q.S.) and center shift (C.S.) are somewhat large or small, respectively, in comparison to those at 295 K, which may be ascribed to ordi-

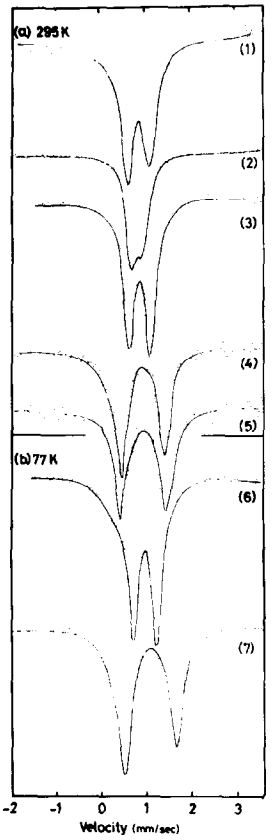

FIG. 3. Mössbauer spectra of typical Fe–Nb–S compounds at 295 K and 77 K. (1) 2s–$(Fe_{1/10}Nb_{9/10})_{1.234}S_2$, (2) 2s–$(Fe_{1/5}Nb_{4/5})_{1.252}S_2$, (3) 2s–$(Fe_{1/3}Nb_{2/3})_{1.382}S_2$, (4) 2s–$(Fe_{1/3}Nb_{2/3})_{1.5}S_2$, (5) 2s–$(Fe_{1/3}Nb_{2/3})_{1.515}S_2$, (6) is (3) at 77 K, and (7) is (4) at 77 K.

nary temperature dependence. All the samples with iron content $y \leq 1/3$ are therefore paramagnetic down to 77 K, consistent with results of the magnetic susceptibility measurement of 2s–$Fe_{1/3}NbS_2$ ($x = 1/3$, $y = 1/4$) reported by Anzenhofer *et al.* (*5*). Figures 4 and 5 show the Q.S. and the C.S. of the spectra taken at 295 K plotted vs x. Both the Q.S. and C.S. increase with increasing x and decreasing y. The values of the C.S. fall in a range of $1.0 \sim 0.82$ mm/sec relative to 310 stainless steel, which are typical values for the high spin Fe^{2+} ions in the sulfides, and the 4s electron contribution is estimated at about $15 \sim 20\%$ from Walker's chart (*13*). The divalent state of the iron atoms has already been proposed for 2s–$Fe_{1/3}NbS_2$ ($x = 1/3$, $y = 1/4$) by Anzenhofer *et al.* (*5*) from susceptibility and Mössbauer measurements. It is worth noting that, as seen in Fig. 4, the Q.S. depends strongly on the values of x and y. This may be interpreted as follows: Fig. 6 shows the Q.S. for all the prepared compositions plotted as a function of the ratio $c/2a$. The Q.S. increases steadily with increasing $c/2a$, and so is closely related to lattice elongation along the c axis. According to Anzenhofer *et al.*, the larger the value of $c/2a$, the larger the distortion of sulfur octahedrons between the NbS_2 layers in the 2s–$(M_{1/4}Nb_{3/4})S_2$ system (M = Mn, Fe, Co, Ni), and a similar phenomenon should also occur in the $(Fe_yNb_{1-y})_{1+x}S_2$ system. Since the 3d transition metal intercalated into the host NbS_2 structure is believed to enter the octahedral interstices, the Q.S. observed for the present 2s–$(Fe_yNb_{1-y})_{1+x}S_2$ system may be attributed to the distortion of the octahedrons which enhanced on increase of $c/2a$. As shown in the insets of Figs. 4 and 5, the Q.S. and the C.S. of the system for which y

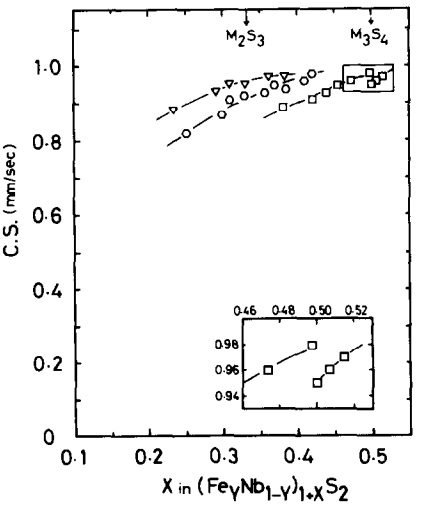

FIG. 4. Plot of center shift vs x in $(Fe_yNb_{1-y})_{1+x}S_2$.

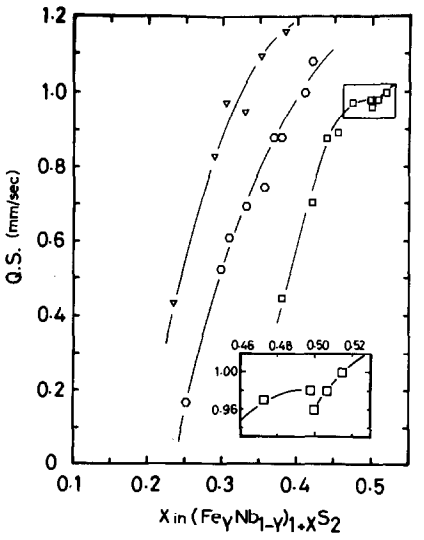

FIG. 5. Quadrupole split and composition variation of the Fe–Nb–S system.

= 1/3 show a slight discontinuity at x = 0.50.* A slight discontinuous change at x = 0.50 is also found in the lattice parameters of the same system, as seen in Fig. 2. Some possible models for the distribution of guest cations in the interstitial layers of the 2s–$(Fe_yNb_{1-y})_{1+x}S_2$ system ($0 \leq x, y \leq 1$) are proposed to account for these discontinuities.

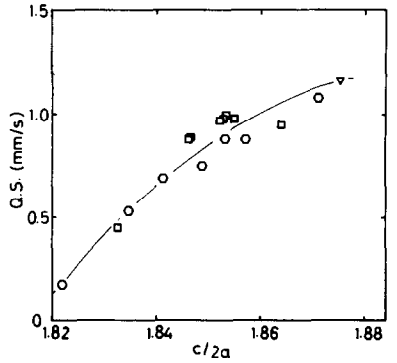

FIG. 6. Plot of quadrupole split vs ratio of lattice parameters, $c/2a$.

* The mean deviations are estimated as ±0.015 mm/sec for the C.S. and ±0.02 for the Q.S., which are smaller than the discontinuity.

Proposed models

Since in 2s–$Nb_{1+x}S_2$ with x = 0 every other metal layer is completely vacant and the unit cell in the c-direction consists of two S–Nb–S slabs and two van der Waals gaps, there are three possible stackings of prismatic layers. The corresponding stackings and the hexagonal (11$\bar{2}$0) planes of the 2s–NbS_2 are shown in Figs. 7a and b, respectively. Jellinek (*14*) proposed that 2s–$Nb_{1+x}S_2$ belongs to type (i) in Fig. 7 from examining the crystal structures of various sulfides, and later, Van Den Berg *et al.* (*4*) and Anzenhofer *et al.* (*5*) confirmed his results. In addition, type (ii) was found for 2s–MoS_2 (*14, 15*), and type (iii) for 2s–$NbSe_2$ (*16*). The principal crystal structure of 2s–$Nb_{1+x}S_2$ at x = 0 is shown in Fig. 8.

On preparing the iron niobium sulfides with y = 1/3 (2s–$(Fe_{1/3}Nb_{2/3})_{1+x}S_2$) at 950°C, we obtained samples with x from 0.38 to 0.52 as shown in Table I. At x > 0.52, the 2s–$(Fe_{1/3}Nb_{2/3})_{1+x}S_2$ decomposed. This series of sulfides enabled us to surmise how iron or niobium ions enter into the van der Waals gaps between the S–M–S slabs. Let us divide the composition series of the 2s–$(Fe_{1/3}Nb_{2/3})_{1+x}S_2$ into the following three cases, i.e., x = 0.5, x < 0.5, and x > 0.5. At x = 0.50 (2s–$Fe_{1/2}NbS_2$), two possi-

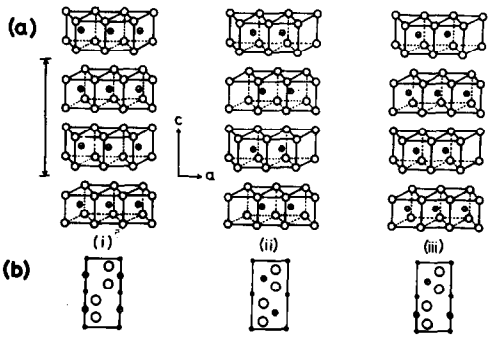

FIG. 7. (a) Three kinds of stacking of prismatic coordination. Arrow: length of unit cell in the c-direction. (b) Corresponding hexagonal (11$\bar{2}$0) planes. Shaded circles, metals; black circles, octahedral interstices; open circles, sulfur.

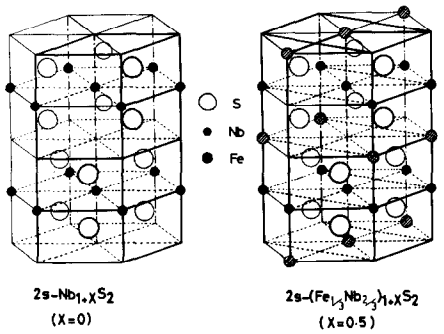

FIG. 8. Crystal structures of $2s\text{–}(Fe_{1/3}Nb_{2/3})_{1.5}S_2$ ($2s\text{–}Fe_{1/2}NbS_2$) and $2s\text{–}Nb_{1+x}S_2$.

ble iron ion distributions between the S–Nb–S slabs could be considered from the Mössbauer spectra of a single quadrupole splitting ((3) and (6) in Fig. 3). The principal slabs and the two iron distribution models at $x = 0.5$ are illustrated in Figs. 9a, b, and b'.

In model (b) the iron atoms are intercalated into every van der Waals gap in equal amounts. In model (b'), all the iron atoms are intercalated in every other originally completely vacant metal layer until they fill up all the metal sites in those layers. Model (b') may be that the iron atoms initially occupy more distant van der Waals gaps lowering the repulsion between positive layers as pointed out by Rouxel *et al.* (*17*) for some alkali metals. However, in the X-ray powder diffraction pattern of the $2s\text{–}Fe_{1/2}NbS_2$, we did not find any peak of (001) near $2\theta \simeq 11°$ ($CrK\alpha$), which can be observable when every other vacant layer exists. This means that model (b) is preferable.

The order–disorder problems in the metal layers of the iron niobium sulfides have been investigated by Anzenhofer *et al.* (*5*) (X-ray diffraction using single crystal), Boswell *et al.* (*8*), and Tendeloo *et al.* (*9*) (electron microscopy). They suggested that the iron ions occupying octahedral interstices in every van der Waals gap form $a\sqrt{3}$ superlattice in the intralayers. According to Tendeloo *et al.* (*9*) the ordering is affected by the quenching rate. From the X-ray diffraction patterns of our quenched powder samples we could not observe any clear peaks of the superstructures described by Voorhoeve *et al.* (*18*) for

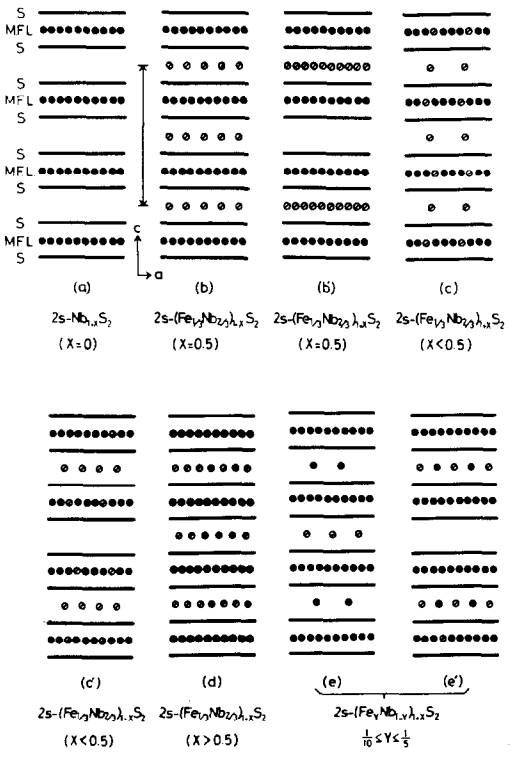

FIG. 9. Proposed models for cation distribution in metal layers of iron niobium sulfides prepared in the present study. The arrow indicates the length of the lattice constant c in the $2s\text{–}Nb_{1+x}S_2$ superstructure.

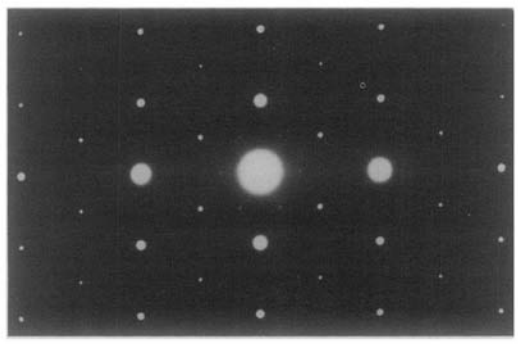

FIG. 10. Observed electron diffraction pattern for $Fe_{1/2}NbS_2$.

$Fe_{1/2}NbSe_2$. To reconfirm these results we took the electron micrographs and the electron diffraction pattern of the 2s–$Fe_{1/2}NbS_2$ obtained in the present study. The diffraction pattern is shown in Fig. 10. At this composition the crystal exhibited strong $a\sqrt{3}$ superlattice spots as already pointed out in the literature (*5, 8, 9*), and each atom seems to be in ordered state. From these considerations the principal crystal structure for 2s–$(Fe_{1/3}Nb_{2/3})_{1+x}S_2$ at $x = 0.5$ (2s–$Fe_{1/2}NbS_2$) based on model (b) may be surmised as shown in Fig. 8. Another expression of the same cation distribution for the 2s–$Fe_{1/2}NbS_2$ based on model (b) is also shown in Fig. 11a; here, the orthorhombic unit cell ($a = 2a_0, b = 2\sqrt{3}a_0, c = 2c_0$) is taken for easy understanding. Linear Nb–Fe–Nb groups give rise to a zigzag-like pattern in the c-direction.

Models (c) and (c′) in Fig. 9 refer to x smaller than 0.5. In this region of x, the number of niobium atoms is not enough to fill up an originally metal-filled layer to keep the essential 2s–$Nb_{1+x}S_2$ type structure. Therefore, the iron atoms should move from other partially filled metal layers to the original metal-filled layers until full occupation of the metal sites by Nb and Fe atoms in the metal-filled layers is attained. For reasons similar to those described above, we propose that model (c) may be more accurate than model (c′), and accordingly, originally metal-empty layers would permit insertion of an equal amount of iron atoms in each alternate metal layer. The cation distribution in each metal layer calculated for reliable models is given in Table II. The Mössbauer spectra exhibit a single quadrupole splitting ((3) and (6) in Fig. 3), in spite of intercalation of iron atoms into two kinds of layers. Although the iron amount in the originally metal-filled layer is rather smaller (less than 7.9% in Table II) than that of the partially filled layer, it may be that the iron atoms in both layers are subject to some similar electronic property when the iron atoms intercalate. Of course if we could use an apparatus with high resolving power, some slight difference in the iron atom behavior might be sufficient to distinguish the alternate layers.

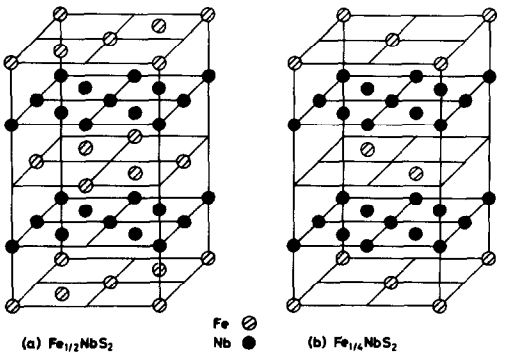

FIG. 11. Cation distributions in each metal layer: (a) for $Fe_{1/2}NbS_2$, and (b) for $Fe_{1/4}NbS_2$. Sulfur atoms are omitted. Each metal layer corresponds to that in Fig. 8.

For $x > 0.5$ in 2s–$(Fe_{1/3}Nb_{2/3})_{1+x}S_2$, only one possible model exists, model (d) shown in Fig. 9. Excess metal over $x = 0.5$ will enter into equivalent partially filled layers, but the maximum solubility in the layers is only 1.5% (Table II). We found several anomalies at $x = 0.5$ for 2s–$(Fe_{1/3}Nb_{2/3})_{1+x}S_2$ in the present experiments. As a possible reason for such behaviors, we suppose that the iron and niobium atoms which would have alternate states with each outer electron having different site preference energies have to enter the same partially filled layer over $x = 0.5$. More intercalation in the partially filled layer results in the breakage of the 2s–$Nb_{1+x}S_2$ structure.

In the case of 2s–$(Fe_{1/5}Nb_{4/5})_{1+x}S_2$ or 2s–$(Fe_{1/10}Nb_{9/10})_{1+x}S_2$, where metallic ratio $y < 1/3$, two models (e) and (e′) may be considered. In model (e), the originally metal-filled layer is occupied by the niobium atoms and the remaining niobium and iron atoms are introduced into the other depleted layers separately. In another model (e′), the niobium and the iron atoms enter

TABLE II

CATION DISTRIBUTION BASED ON THE PROPOSED MODELS FOR IRON NIOBIUM SULFIDES PREPARED AT 950°C[a]

Model	X in $M_{1+x}S_2$	p.f.l.(I) Fe(%)	p.f.l.(I) Nb(%)	p.f.l.(II) Fe(%)	p.f.l.(II) Nb(%)	m.f.l. Fe(%)	m.f.l. Nb(%)
			$2s\text{–}(Fe_{1/3}Nb_{2/3})_{1+x}S_2$				
Model (d)	0.515	50.5	1.0	—	—	0	100
	0.507	50.2	0.5	—	—	0	100
Model (b)	0.500	50.0	0	—	—	0	100
Model (c)	0.498	49.8	0	—	—	0.1	99.9
	0.473	47.3	0	—	—	1.8	98.2
	0.455	45.5	0	—	—	3.0	97.0
	0.440	44.0	0	—	—	4.0	96.0
	0.421	42.1	0	—	—	5.3	94.7
	0.382	38.2	0	—	—	7.9	92.1
			$2s\text{–}(Fe_{1/5}Nb_{4/5})_{1+x}S_2$				
Model (e)	0.421	56.8	0	0	27.4	0	100
	0.409	56.4	0	0	25.4	0	100
	0.386	55.4	0	0	21.8	0	100
	0.370	54.8	0	0	19.2	0	100
	0.357	54.3	0	0	17.1	0	100
	0.329	53.2	0	0	12.6	0	100
	0.310	52.4	0	0	9.6	0	100
	0.300	52.0	0	0	8.0	0	100
	0.252	50.1	0	0	0.3	0	100
			$2s\text{–}(Fe_{1/10}Nb_{9/10})_{1+x}S_2$				
Model (e)	0.383	27.7	0	0	48.9	0	100
	0.362	27.2	0	0	45.2	0	100
	0.352	27.0	0	0	43.4	0	100
	0.350	27.0	0	0	43.0	0	100
	0.340	26.8	0	0	41.2	0	100
	0.330	26.6	0	0	39.4	0	100
	0.309	26.2	0	0	35.6	0	100
	0.291	25.8	0	0	32.4	0	100
	0.234	24.7	0	0	22.1	0	100

[a] p.f.l. indicates the partially metal-filled layer; m.f.l. the originally metal-filled layer.

into every other vacant metal layer and occupy the available metal sites. Thus, the depleted layers remain in a completely empty state. In considering the reliability of models (e) and (e′) in this composition range, model (e) may be selected as the reasonable one, because (i) iron and niobium atoms having different site preference energies may enter into separate layers as far as they can, and (ii) no relic (001) peak of X-ray diffraction pattern was found for the quenched samples in these composition ranges. (The model (e′) would be supported by the existence of the any appreciable peak (001).) Moreover, the $2s\text{–}(Fe_{1/10}Nb_{9/10})_{1+x}S_2$ compounds contained small amounts of the rhombohedral $3s\text{–}Nb_{1+x}S_2$ type structure at $x < 0.23$. As a qualitative explanation, the activation energy of the transformation from the $2s\text{–}Nb_{1+x}S_2$ to the $3s\text{–}Nb_{1+x}S_2$ would be less in model (e) than model (e′). The cation distri-

bution calculated for model (e) is given in Table II. As a typical example, the positions of each cation based on model (e) of the 2s–$Fe_{1/4}NbS_2$ (2s–$(Fe_{1/5}Nb_{4/5})_{1+x}S_2$; x = 0.25) is shown in Fig. 11b. The symmetry in the iron layer in the $Fe_{1/4}NbS_2$ is better than that of $Fe_{1/2}NbS_2$. This may also contribute to the rapid decrease in the Q.S. (Fig. 5).

Acknowledgments

The authors express their thanks to Prof. M. Nakahira, Prof. S. Nomura, and Dr. M. Onoda for fruitful discussions, Prof. M. Yoshida for presentation of natural pyrite, and Prof. T. Takahashi, Prof. K. Mihama, and Dr. T. Sato for taking electron micrographs and electron diffraction spots. Part of this study was supported by a Grant-in Aid for Scientific Research from the Ministry of Education of Japan.

References

1. M. S. WHITTINGHUM, *Progr. Solid State Chem.* **12,** 41 (1978).
2. W. P. F. A. M. OMLOO AND F. JELLINEK, *J. Less Common Metals* **20,** 121 (1970).
3. M. EIBSCHÜTZ, E. HERMON, AND S. SHTRIKMAN, *Acta Crystallogr.* **22,** 944 (1967).
4. J. M. VAN DEN BERG AND P. COSSEE, *Inorg. Chim. Acta* **2,** 143 (1968).
5. K. ANZENHOFER, J. M. VAN DEN BERG, P. COSSEE, AND J. N. HELLE, *J. Phys. Chem. Solids* **31,** 1057 (1970).
6. J. ROUXEL, A. LE BLANC, AND A. ROYER, *Bull. Soc. Chim. Fr.* **6,** 2019 (1971).
7. A. LE BLANC-SOREAU, J. ROUXEL, M. F. GARDETTE, AND O. GOROCHOV, *Mat. Res. Bull.* **11,** 1061 (1976).
8. F. W. BOSWELL, A. PRODAN, W. R. VAUGHAN, AND J. M. CORBETT, *Phys. Stat. Sol. (a)* **45,** 469 (1978).
9. G. VAN TENDELOO, R. DE RIDDER, L. VAN GOETHEM, D. VAN DYKE, J. VAN LANDUYT, AND S. AMELINCKX, *Phys. State. Sol. (a)* **42,** 319 (1977).
10. K. TATSUKI, M. WAKIHARA, AND M. TANIGUCHI, *J. Less Common Metals* **68,** 183 (1979).
11. M. WAKIHARA, T. UCHIDA, AND M. TANIGUCHI, *Mat. Res. Bull.* **11,** 973 (1976).
12. F. KADIJK AND F. JELLINEK, *J. Less Common Metals* **19,** 421 (1969).
13. L. R. WALKER, G. K. WERTHEIM, AND V. JACCARINO, *Phys. Rev. Lett.* **6,** 98 (1961).
14. F. JELLINEK, *Arkiv. Kemi* **20,** 447 (1964).
15. F. JELLINEK, G. BRAUEL, AND H. MÜLLER, *Nature (London)* **185,** 376 (1960).
16. R. HUISMAN, F. KADIJK, AND F. JELLINEK, *J. Less Common Metals* **12,** 423 (1967).
17. J. ROUXEL, T. TRICHET, P. CHEVALIER, P. COLOMBET, AND O. A. GHALOUN, *J. Solid State Chem.* **29,** 311 (1979).
18. J. M. VOORHOEVE, NÉE VAN DEN BERG, AND M. ROBBINS, *J. Solid State Chem.* **1,** 134 (1970).